NANO REVIEW

Drying nano particles solution on an oscillating tip at an air liquid interface: what we can learn, what we can do

Charlotte Bernard · Jean-Pierre Aimé · Sophie Marsaudon · Raphaël Levy ·
Anne Marie Bonnot · Cattien Nguyen · Denis Mariolle · François Bertin ·
Amal Chabli

Abstract Evaporation of fluid at micro and nanometer scale may be used to self-assemble nanometre-sized particles in suspension. Evaporating process can be used to gently control flow in micro and nanofluidics, thus providing a potential mean to design a fine pattern onto a surface or to functionalize a nanoprobe tip. In this paper, we present an original experimental approach to explore this open and rather virgin domain. We use an oscillating tip at an air liquid interface with a controlled dipping depth of the tip within the range of the micrometer. Also, very small dipping depths of a few ten nanometers were achieved with multi walls carbon nanotubes glued at the tip apex. The liquid is an aqueous solution of functionalized nanoparticles diluted in water. Evaporation of water is the driving force determining the arrangement of nanoparticles on the tip. The results show various nanoparticles deposition patterns, from which the deposits can be classified in two categories. The type of deposit is shown to be strongly dependent on whether or not the triple line is pinned and of the peptide coating of the gold nanoparticle. In order to assess the classification, companion dynamical studies of nanomeniscus and related dissipation processes involved with thinning effects are presented.

Keywords Nanofluidics · Nanoparticles · Micromeniscus · Nanomeniscus · Dynamical mode of atomic force microcopy

Introduction

When a spilled drop of coffee dries on a solid surface, it leaves coffee particles that may form various patterns. Coffee, initially dispersed in water, produces brown stains on the substrate. The behavior of the contact line determines how the coffee will cover the surface. The contact line is the triple line that determines the frontier between gas, solid and liquid. When the contact line slides freely, the coffee is on the whole surface area covered by the initial drop. When the contact line is pinned, a characteristic pattern with a ring like deposit along the drop perimeter is observed. The latter case leads to a power law growth of the ring mass with time that only depends on the pinned behavior of the contact line [1]. Fluid behaviors at micrometer and nanometer scale are likely to be extensively used as ways to assemble nano particles into structures from nanometre to mesoscopic scales. Understanding spreading of nanofluids containing surfactant micelles or functionalized nanoparticles leads to numerous and fundamental questions concerning adhesion, flow rearrangement at the triple line and the influence of liquid confinement [2–8]. In particular, capillary flow on the

C. Bernard · J.-P. Aimé (✉) · S. Marsaudon
Université Bordeaux-1, CPMOH 351 cours de la Libération,
Talence cedex 33405, France
e-mail: jp.aime@cpmoh.u-bordeaux1.fr

R. Levy
Center for Nanoscale Science, Bioscience Building and
Department of Chemistry, University of Liverpool, Liverpool
l69 7zb, UK

Anne M. Bonnot
Institut Néel, CNRS, BP 166, Grenoble Cedex 9 38042, France

C. Nguyen
ELORET Corporation/NASA Ames Research Center, MS 229-1
Moffett Field, Mountain View, CA 94035-1000, USA

D. Mariolle · F. Bertin · A. Chabli
CEA-LETI, MINATEC, 17 rue des Martyrs, Grenoble Cedex 9
38054, France

neighbouring of the contact line may lead to a large stress and peculiar superstructures when driven by evaporation flow. At the proximity of the pinned line evidence of two-dimensional crystal like ordering of nanometre sized polystyrene spheres in water has been shown [6]. Also, using drying processes, ordering of anisotropic nanoparticles, such as axi-symmetric nanorods, is achieved. As expected with anisotropic nano-objects, most of the experiments on self-assembly of nanorods lead to packing in a parallel fashion [7]. However, as shown recently, drying of solution of gold nanorods with covalently attached polystyrene arms allowing solubilization in dichloromethane have given well characterized rings of nanorods. Structure of the ring, in particular ordering of nanorods along the curved triple line appears strongly dependent on nanorods dilution [8]. The result emphasizes the effect of the confinement and the influence of large stresses occurring close to the contact line.

The present work aims at using AFM tips to study nanofluid properties and structure of deposit of gold nanoparticles coated with selected peptide sequences. With the improving capabilities of scanning nanoprobes and the development of AFM dynamical modes, there are new avenues open to investigate and to manipulate a small amount of liquid, typically 10^{-17} L. For instance, phenomena occurring at the triple contact line where liquid confinement occurs can be investigated [9]. The basic idea is to use a micro or nanomeniscus to deposit functionalized nano particles. To do so, we need first to prevent the liquid from a complete wetting. As the geometry of the solid surface has a strong influence on the wetting transition between partial and complete wetting, a curved surface can be used to reduce the wetting. A good example is the wetting of a fiber with a small radius r. A spherical drop, even with a positive spreading coefficient S > 0, may not spread on the fiber [10, 11]. The Laplace pressure γ/r (with γ the liquid surface tension), balances the wetting force and, for small radius r, the precursor film hardly wets a highly curved surface. Therefore AFM tips are suitable to control the liquid spreading.

Evaporation gives the driving hydrodynamic force monitoring the flow of the aqueous solution, in turn the deposit of the coated gold nanoparticles. For a pinned triple line, the meniscus becomes thinner and a constant evaporating flow leads to a drastic increase of the liquid velocity inside the meniscus. The present work describes a method to investigate competitive interactions between the hydrodynamic forces generated through the liquid flow inside the meniscus and the strength of adhesion between the nanoparticles (NP) and the tip. The gold nanoparticles are coated either with peptides able to specifically interact with silica surface or carbon surface. Therefore, the competition between hydrodynamic and adhesion forces can be balanced by varying the sequence of the peptides, in turn change of the meniscus dynamical properties and structure of the deposits.

The paper is organised as follow. In the experimental section the materials used are described, the materials used are described: gold nanoparticles, peptides sequences and carbon tips, and the experimental method is detailed. In the next section, experimental results obtained with hydrophobic conical tips dipped in two different aqueous solutions and tip apex ended with a multi wall carbon nanotube dipped in an aqueous solution are presented. In this section, the differences in structure of the coated gold nanoparticles and of the dynamical properties of the meniscus as a function of the peptides used are emphasized. The section Discussion is a summary attempting to connect hydrodynamic properties of the meniscus and structure of the deposits.

Experimental section: materials and method

Materials

Gold nanoparticles and selected peptide sequences

Materials that combine inorganic components and biological molecules provide a new example for synthesizing nanoscale and larger structures with tailored physical properties. These synthesis techniques utilize the molecular recognition properties of many biological molecules to nucleate and control growth of the nanoscale structure. Phage-displayed peptide libraries are a powerful tool to identify peptides that selectively recognize and bind to a variety of inorganic surfaces that are utilized in electronic and photonic devices.

The gold nanoparticles used in this work were capped with a self-assembled monolayer of peptides as described previously [12]. The design strategy of the peptide initially studied took into account the need to have a strong affinity for gold, ability to self-assemble into a dense layer that excludes water, and a hydrophilic terminus, which would ensure solubility and stability in water. The pentapeptide CALNN (Fig. 1) was designed to achieve these goals. A
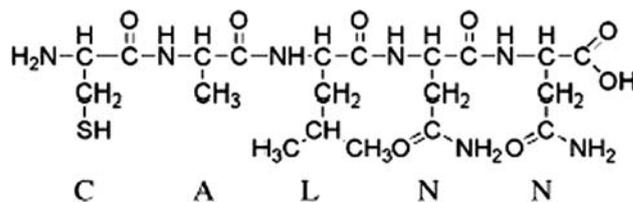

Fig. 1 CALNN structure

detailed description of the oligopeptide properties is given in reference [12].

The introduction of specific recognition groups at the surface of gold nanoparticles is an important prerequisite for their use in bioanalytical assays. In the present case, this is readily achieved by incorporating a proportion of an appropriately functionalized peptide in addition to CALNN in the preparation process. Phage peptide display is a selection technique in which random peptides from a library are expressed as a fusion with a phage coat protein, resulting in a display of the fused protein on the surface of the phage particle. The formula of this silica-bending peptide is CALNNGMSPHPHPRHHHT [13], hereafter noted CALNN-Si-peptide, and the peptide which has a selective affinity for carbon nanotubes is CAL-NNGHWKHPWGAWDTL [14], hereafter noted CALNN-Carbon-peptide. Each selected peptide is mixed with the peptide CALNN previously described in a proportion of 3–100 and then blended with gold nanoparticles of diameter 10 nm in a volume ratio of 1 of 10. These two solutions are then centrifuged and filtered in order to eliminate peptides in excess.

Hydrophobic tip and multi wall carbon nanotube

HFCVD: single wall carbon nanotubes (SWNT) were prepared by Hot Filament assisted Chemical Vapor Deposition (HFCVD). The advantage of the technique is to allow localizing and self assembling of suspended isolated SWNT [15, 16]. The HFCVD apparatus has been built for diamond thin film growth [16]. It appears also to be an appropriate way to coat conical tips with dispersed SWNTs. The catalytic growth of SWNT was obtained thanks to a 1–8 nm thick Co layer deposited by standard evaporation techniques. The vapor was composed of 5–20 vol.% methane proportion in hydrogen. Typical deposition parameters were a 750–850 °C substrate temperature and a 30–100 mbar total pressure. The tungsten filament, placed 1 cm above the substrate, was heated up to 1990–2100 °C. The specificity of this HFCVD technique is to take advantage of this hot tungsten filament to decompose the vapor into active carbon species which react with the catalytic Co surface. It also plays an important role in the cleaning of disordered sp^2 solid carbon phases and thus in the high purity of the SWNT deposit.

MWNT: MWCNT tips are fabricated by manually attaching MWCNT to Si pyramidal tips. Following the initial gluing method of Dai et al. [17], individual MWCNT are fused on Si tips sputtered with Nickel coating [18]. In brief, an inverted optical microscope equipped with two X-Y-Z micro-translators/manipulators is used to control the MWCNT/Si tip relative positionning and a DC field is applied between the MWCNT and the metal coated Si tip to fuse the MWCNT on the tip, ensuring a firm fixing of the MWCNT on the Si tip. The source of MWCNT is obtained by CVD growth on Pt wire using liquid catalyst, ensuring low density of MWCNT on the wire for individual selection ([19]).

Method: dipping process with an oscillating tip

Several cantilevers are used, with quality factors ranging between Q = 300 and Q = 500. The resonant frequencies vary between 150 and 250 kHz. The cantilever stiffnesses are about $k \simeq 30$ Nm^{-1}. The quality factors give experimental bandwidths around 1 ms. Therefore, the experimental data are averaged quantities extracted from several hundred oscillation amplitudes. The great advantage of the experimental procedure is to prevent the cantilever to be fully immersed when the tip oscillates in the liquid. Because only the very end of the tip oscillates in the liquid, the amount of liquid and the viscous damping are greatly reduced. The quality factor of the equivalent harmonic oscillator remains high and a good sensitivity is preserved.

The experiments are done as follows: the AFM tip is approached gently to the air liquid interface with a step motor. When the tip touches the surface, it oscillates in the liquid, and the frequency modulation (FM-AFM) mode is used to record changes of the oscillating properties of the cantilever. With the FM-AFM mode the resonance frequency shift, measuring the conservative force gradient, and the damping coefficient, measuring the dissipative force, are simultaneously recorded [9].

The wetting angle θ gives the shape of the meniscus at proximity of the contact line (Fig. 2).

Values of the wetting angle θ are extracted from the frequency shift measurement. The shift in the resonant frequency is the result of the elastic restoring force of the triple line giving a positive frequency shift. For small oscillation amplitudes, using simple geometrical arguments, the elastic contribution and corresponding force
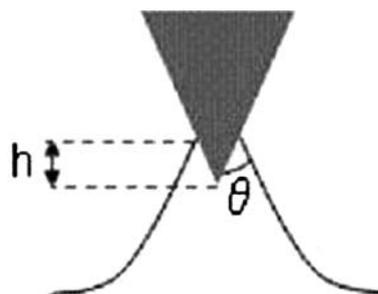

Fig. 2 Scheme of a meniscus on conical tip, with the description of the angle and height of the meniscus as given with Eq. (2)

gradient can be readily calculated, giving the resonant frequency shift

$$\Delta v \sim \frac{\pi}{2} v_0 \frac{\gamma}{k ln(\delta/R)} sin^2\theta \qquad (1)$$

where v_0 is the resonant frequency of the microcantilever, γ the liquid surface tension (Nm^{-1}), k the microcantilever stiffness (also Nm^{-1}), R the radius of curvature of the surface, δ a characteristic length that remains to be defined. Note that compared to the equation given in reference [9], the relationship between the resonant frequency shift Δv and the wetting angle θ is sligthly modified and a simple inversion of the equation 1 gives the wetting angle of the nanomeniscus. This is because the expression of the meniscus height $h\propto Rln(\delta/a)$ has been replaced by [20].

$$h \propto Rcos(\theta)ln(\delta/a) \qquad (2)$$

where a is a molecular length.

About two typical sequences of dipping events in water solution of nanoparticles are shown in Fig. 3.

The liquid is approached with a step motor towards the tip. When the tip is far from the surface, that is, more than a few 10 nm, there is no interaction and thus no frequency shift (phase 1). As soon as the tip touches the liquid, the elastic response of the meniscus induces a positive shift of the resonance frequency (phase 2). Because of the water evaporation, the average contact angle decreases with time leading to a decrease in the frequency shift (phase 3). The phase 4 noted is identical to the phase 1 with no significant interaction between the tip and the liquid.
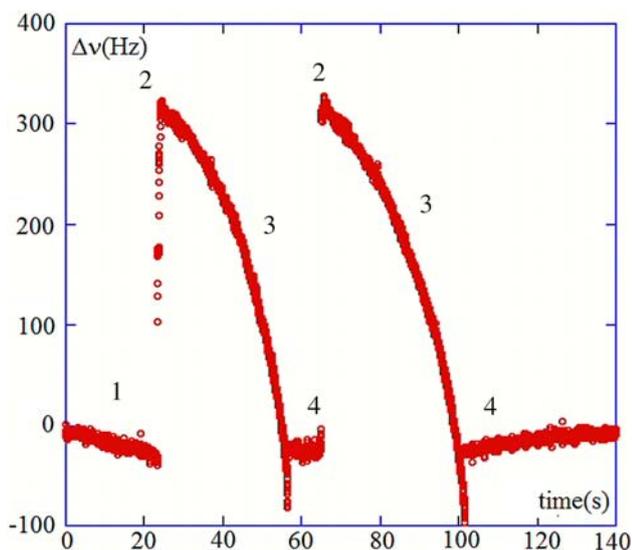
Experimental results

First, the tips employed in the dipping experiments were covered with amorphous carbon produced with chemical vapor deposition using a hot tungsten filament. The conical tips coated with carbon give them a hydrophobic property that prevents from a complete wetting. When silicon tips with the same size are used, the dipping of the tip cannot be controlled and, most often, leads to a complete wetting that may also include the cantilever itself. The height of the meniscus scales as the product of the radius of the surface with a logarithm coefficient. Thus the meniscus height is around 2 μm, and the radius of the tip at the vertical location of the ring structure (Figs. 4 and 5) is about the micrometer size. As the capillary force is proportional to the radius $F_{cap} \sim \gamma 2R$, it can be large enough to reach 100 nN.

Much lower capillary forces are present when nano-needles or multi wall carbon nanotubes are used. In the present work, the second type of tip is ended with a multi wall carbon nanotube of diameter 20 nm. In latter case, the experiments were an attempt to finely control the dipping of a multi wall nanotubewith the main objective to stick the functionalized gold NP on it.

Oscillating carbon conical tip at the air liquid interface: case of an aqueous solution of nanoparticles coated with CALNN-Si-Peptide

We focus first on experimental results corresponding to dipping in solution of gold nanoparticles covered with CALNN-Si-peptide.

Fig. 3 Variations of the resonance frequency shift as a conical tip covered with carbon dips in a solution of gold NP-CALNN-Si-peptide (see text)
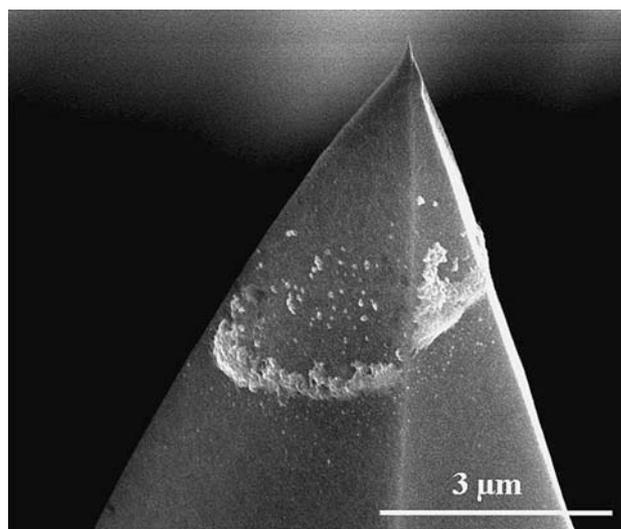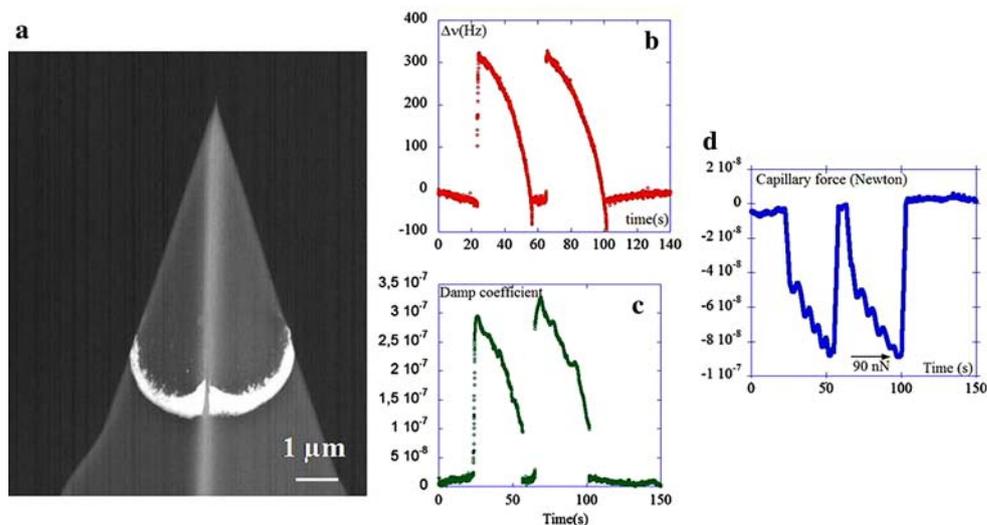

Fig. 4 Conical tip covered with cobalt film (thickness 7 nm) and carbon after dipping in an aqueous solution of coated nanoparticles with CALNN-Si-peptide

Fig. 5 Structure of a tip dipped in solution with gold nanoparticles coated with CALNN-Si-peptide. The conical tip was covered with cobalt film of thickness 1 nm and amorphous carbon deposited with HFCVD before dipping experiments. The height of the meniscus is $h = 2$ μm

The image (Fig. 4) corresponds to dipping of a conical tip covered with amorphous carbon using the HFCVD method. The initial thickness of the Cobalt is about 7 nm. The tip was dipped in solution of nanoparticles coated with Si-oligopeptide, thus a peptide that does not have any specific interaction with carbon tips. The image shows the formation of a ring of nano particles located at 2 μm from the apex. The ring is not well organized, the structures indicate a distribution of aggregates and holes, with a fluctuation in size of the width all around the cone. As a result, the structure of the ring is ill defined. All over the tip, there is also evidence of a porous structure of the carbon and cobalt film. The porous structure may in part be issued from a partial dewetting of the cobalt film. Therefore, the thickness of the Co catalytic layer appears to be a relevant parameter to determine the roughness of the substrate. To enhance the quality of the growth of single and double walled carbon nanotube at a tip apex, it was also shown that such a film thickness of the Cobalt film was too large to make efficient and reproducible growth of carbon nanotubes.

An attempt to improve the role of the Co catalytic layer is to use a thinner film of Cobalt. For instance, the use of a film thickness of 1 nm has proven to be efficient in improving the growth of single wall carbon nanotube. Therefore, conical tips covered with a Cobalt thickness of 1 nm were also used for the dipping experiments. The MEB image is displayed in Fig. 5a, the image shows an homogeneous coating of the tip with no evidence of holes induced with a dewetting of the film. As shown in the figure, after the tip was dipped in the solution with NP and CALNN-Si-peptide, a well defined ring structure is observed. The two images, 4 and 5, illustrate the influence of the structure of the initial film made of cobalt and

carbon. The roughness of the tip has a marked effect on the liquid wetting and nanoparticles patterning.

Recording changes of cantilever configuration during the dipping process helps to better understand the interaction between the nanoparticles and the tip. In addition, the frequency shift and damping curves must provide an immediate information concerning the attachment of nano particles on the tip. Companion experimental curves showing the resonant frequency shift variation, the damping and the capillary forces are displayed in Fig. 5b, c and d respectively.

With the conical tips, the strength of the hydrodynamic forces produced by the meniscus leads to much greater change of the oscillation properties than those observed with the nanoneedles [9].

For instance, with several tenth of seconds, the dipping times are an order of magnitude larger than the dipping times measured with a nanoneedle [9]. This is a direct consequence of the large size of the meniscus. With nanoneedles of small diameter, say 20 nm, the capillary forces are weak with values around 0.1 nN. Such a force leads to cantilever deflections within the picometer range, which are hardly measurable. With a conical tips and a meniscus height of 2 μm, the diameter is almost two orders of magnitude larger leading to measurable cantilever deflections. At the end of the evaporation, when the meniscus burns out, the wetting angle θ is close to zero. Therefore, because the capillary force varies as $f_{cap} \sim \gamma R \cos(\theta)$, at the very end of the evaporation, the capillary force reaches its maximum value of about 100 nN. As display in Fig. 5d, the capillary force reaches a value of 90 nN corresponding to the well defined ring structure shown in Fig. 5a.

At the beginning, the maximum contact angle value is close to 1.3 radians. Such a high value of the wetting angle

may be explained with the hydrophobic coating of the tip. Then, the value goes down to zero value, corresponding to a fully extended meniscus before it breaks.

Oscillating carbon conical tip at a air–liquid interface: case of aqueous solution of nanoparticles coated with CALNN-Carbon-peptide

With a solution of NP-CALNN-Carbon-peptide, the strength of the interaction between the NP and the carbon coated conical tip is improved. Then, question raises on the capability of the adhesion force to overcome laminar flow. Figure 6 shows the deposit of nano particles after dipping twice the tip in the solution. As compared to the use of NP-CALNN-Si-peptide solution (Fig. 5), the obvious difference is an homogeneous covering of the tip. A frontier is still observed, but the frontier is not as marked as it was with the ring structures. However, the frontier line can be used to deduce a meniscus height. The height is $h = 600$ nm, much smaller than the ones shown in Figs. 4 and 5 with heights $h = 2\mu m$.

As compared to the preceeding structures there are three noticeable differences with :

a   the nano particles are distributed all over the wet part of the tip,
b   the height of the meniscus is much smaller,
c   there is no evidence of a strong pinned triple line leading to a marked frontier with a ring structure.

A small height of the meniscus and a weak pinned triple line lead to change on the dynamical behavior of the meniscus. With an evaporating liquid, a weak pinning of the triple line, or a sliding triple line, reduces the life time of the meniscus and gives a smaller dipping time. Figures 6b–d display the whole characteristic of the meniscus dynamical behavior corresponding to the distribution of NP on the tip apex shown in Fig. 6a.
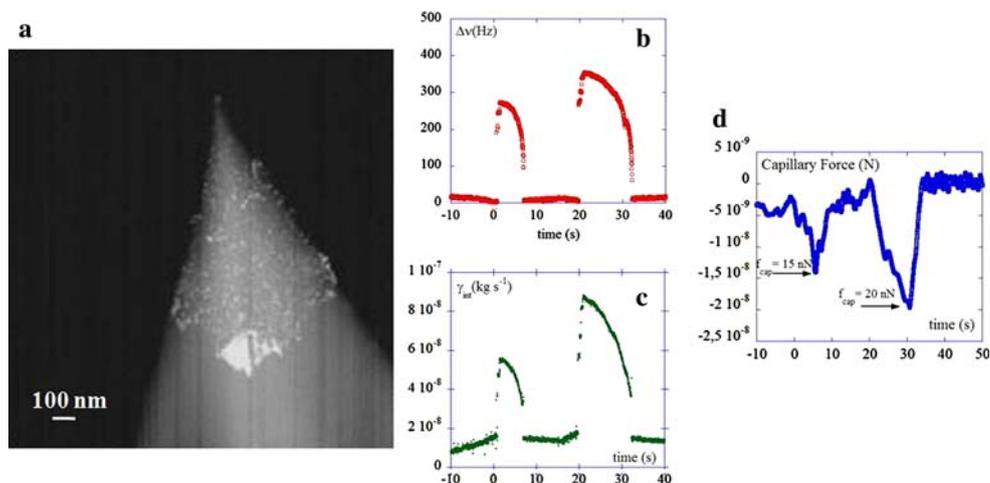
For the two events shown in Fig. 6b, the meniscus breaks before the wetting angle θ reaches a zero value. For a triple contact line partly sliding, the tip leaves the air liquid interface at a finite θ value.

The damping curves (Fig. 6c) give variations of the damping coefficient with values which are one order of magnitude smaller than the ones corresponding to the ring structure (Fig. 6c). Here again, this result can be considered as evidence that the triple line is weakly pinned or not pinned at all. When the triple line is pinned, at a constant evaporating flow, the thinning of the meniscus leads to a diverging liquid velocity inside the meniscus, thus a strong increase of the viscous dissipation. When the triple line is allowed to slide, such a viscous effect is much less important (ref: [21] and discussion below).

The capillary force corresponding to dipping in the solution of NP-CALNN-Carbon-peptide is also much smaller, about five times smaller (see Figs. 5d and 6d). However, the wetting angle θ remains roughly the same as shown in the Fig. 7 comparing the two values computed from the resonance frequency shift variations according to Eq. (1).

However, not all the carbon tips show the same covering of NP-CALNN-Carbon-peptide. More complex processes may also happen giving a mixing of homogeneous covering and ring structures [21].

Oscillating multi wall carbon tip at the air liquid interface : case of solution of nanoparticles coated with CALNN-Carbon-peptide

This part of work is an attempt to biologically functionalize a multi wall nanotube with controlled dipping in a solution of nanoparticles coated with CALNN-Carbon-peptide (Fig. 8). As shown with the arrows in Fig. 8a, there are evidence of nanoparticles stuck on the MWNT.

The diameter of MWCNT being much smaller, about 20 nm, the mass of liquid involved in the meniscus is
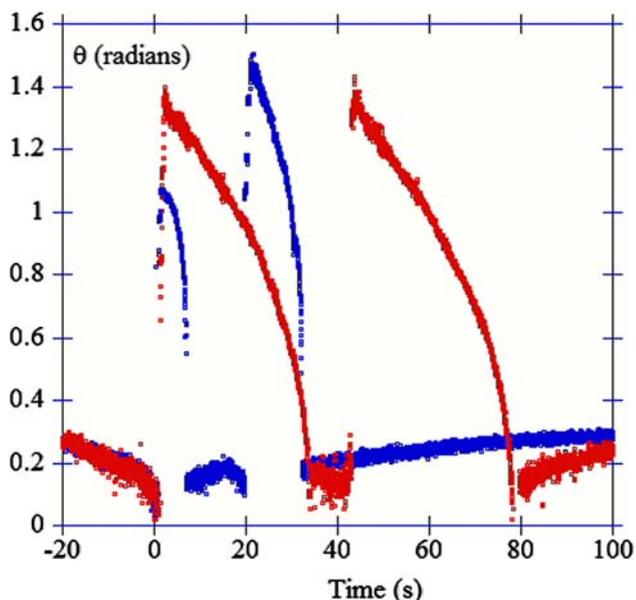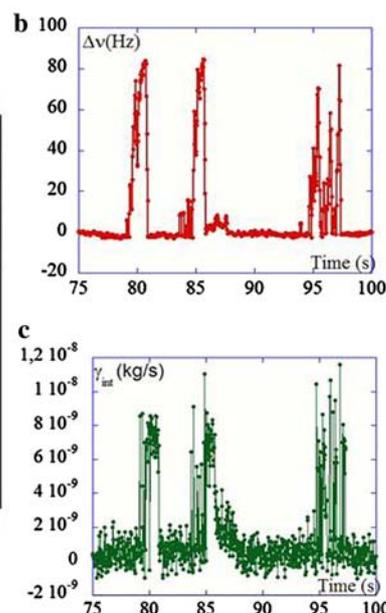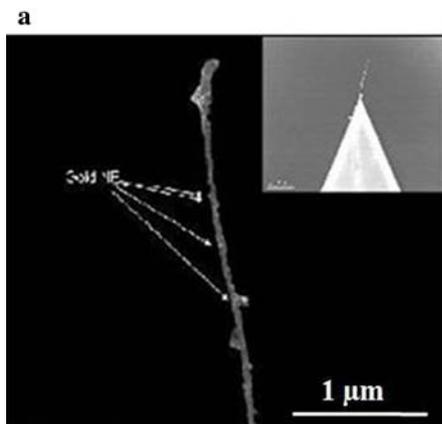

Fig. 6 Image of a hydrophobic, carbon coated, conical tip, after dipping in a solution of NP-CALNN-Carbon-peptide

Fig. 7 Variation of the wetting angle θ for the two dipping experiments shown in Figs. 5 (red symbols) and 6 (blue symbols). For a weakly pinned triple line, the dipping time is shorter and there is an instabilty with a θ value jumping to zero (curves with blue symbols)

several orders of magnitude smaller than the one involved in meniscus with conical tip. There are experimental evidence that for such a smaller diameter the height of the meniscus is no higher than 100 nm [21]. As shown in Fig. 8a, several dipping events were successful in attaching several gold nanoparticles coated with CALNN-C-peptide. However, there is also evidence that oligopeptides without gold NP were also interacting with the nanotube.

The magnitude of the resonance frequency shift is weaker and noisy. Typical variation including three dipping events are shown in Fig. 8b. The corresponding variations of the damping coefficient are shown in Fig. 8c. The wetting angle θ has values lower than the one measured with conical tips, about 0.9 radians, with almost no variations until the meniscus breaks as we may expect from the observed weak variation of the resonant frequency shift (Fig. 8b). Both the constant values of frequency shift and the low dipping time indicate a sliding behavior of the triple contact line along the carbon nanotube wall. This may be explained with the fact that the CNT wall is atomically flat, so that the triple line cannot be pinned on it. The θ value is half the one observed with the conical tip which is partly due to geometrical effect corresponding to the wetting of a conical tip as compared to a tube.

The damping coefficient (Fig. 8c) is an order of magnitude smaller than those observed with carbon conical tips, typically less than $\gamma_{int} \simeq 10^{-8}$kg/s. This result is fully consistant with previous remarks and again indicates a much weaker contribution from the hydrodynamic forces.

Discussion: Thinning process and evaporation inducing 2-D crystal arrangement of nanoparticles

The low viscosity of water leads to weak dynamical non linear effects, thus the dynamic contact angle θ_d keeps values close to the static equilibrium one θ_e. However, when the fluid evaporates, the nanomeniscus properties may become strongly dependent on the rate of evaporation. In particular, when the triple contact line remains pinned at

Fig. 8 MEB image of (**a**) MWNT after several dipping in an aqueous solution of gold nanoparticles coated with CALNN-Carbon-peptide. Arrows indicate the location of some of the attached NP. (**b**) and (**c**) are the corresponding frequency shift and dissipation coefficient. The capillary force is to weak to produce a measurable DC signal

a fixed vertical location on a nanoneedle or a conical tip, several additional effects have to be taken into account.

a- For a fixed vertical location of the contact line, the downard motion of the liquid air interface induces a thinning of the meniscus until it breaks. The process can be seen as an imposed vertical displacement of the contact line.

b- Evaporation leads to an additional velocity in the liquid.

c- Because of the resulting high velocity of the liquid inside the meniscus, when the triple line is pinned, hydrodynamic flow may force growth of nanoparticles 2-D crystallization.

Imposed vertical displacement and nanomeniscus thinning process

Evaporation leads to a large number of physical effects [1]. Those physical effects contain several unknown parameters as the curvature of the air water interface, change of the local temperature and the resulting structure of the heat flow. In reference [1] evaporation of a drop was considered with a detailed analysis of the hydrodynamic flows within the droplet. The latter are responsible for the circular deposit formation when the contact line is pinned. Thus capillary flow was considered as the primary cause of ring stains formation at the contact line during drying of the drop. Similar approach can be readily applied to evaporating meniscus when the contact line remains anchored. We need first to find the evaporative flux J, the flow velocity v is then determined. Near the interface the air is saturated with vapour, as the air at infinity is not saturated the vapour diffuses outward. Using the saturated pressure at the air liquid interface, we start with the Darcy law, from which the evaporating flow is derived:

$$J = \frac{1}{n_l k_B T} D \nabla P_{sat} \qquad (3)$$

where D is the diffusion coefficient in air, P_{sat} the saturated pressure at the air liquid interface, n the density number, $k_B T$ the thermal energy. With the values

$n = 3.3 \times 10^{28}/\text{m}^3$, $k_B T = 4.21 \times 10^{-21}$,
$D = 2 \times 10^{-5} \text{m}^2 s^{-1}$, $P_{sat} = 3 \times 10^3 \text{Nm}^{-2}$.

For low ambient humidity, the pressure gradient is estimated as the ratio of the saturated vapor pressure (at the air water interface) to the shortest distance of the meniscus. The shortest distance may be estimated as being at a very

close proximity of the contact line. Say the smallest thickness of the meniscus is $t = 10$ nm, the calculated flow is

$$J \sim \frac{1}{n_l k_B T} D \frac{P_{sat}}{t} = \frac{10^{-12}}{7} \frac{3 \times 10^3}{10^{-8}} = \frac{3}{7} 10^{-1} \sim 4.2 \text{cm/s}$$

This velocity is high, and even larger than the tip velocity. Typically, for an oscillation amplitude of $A = 10$ nm and a resonance frequency of $v_0 = 150$ kHz the tip velocity is $v = A\omega \sim 1$ cm/s. Therefore, when the triple contact line is pinned and the meniscus becomes very thin, the additional viscous dissipation increases significantly and may even leads to diverging behaviors [9, 20, 21]. On the contrary, when the contact line slides, the meniscus thickness remains large and the liquid speed inside the meniscus remains low. Consequently the viscous damping must be much smaller with a sliding line than with a pinned line. When ring structures are observed, the viscous damping is an order of magnitude higher than the one corresponding to a more regular covering of the tip (Figs. 5c and 6c).

A more accurate structure of the flux J is found by solving an equivalent electrostatic problem, wherein the concentration ϕ_{sat}, respectively the saturated pressure P_{sat} is an electrostatic potential and the meniscus, with its fixed potential, is a conductor with a neck shape. Singular behavior occurs at the contact line leading to diverging flux at proximity of the contact line (reference [1] and Fig. 9):
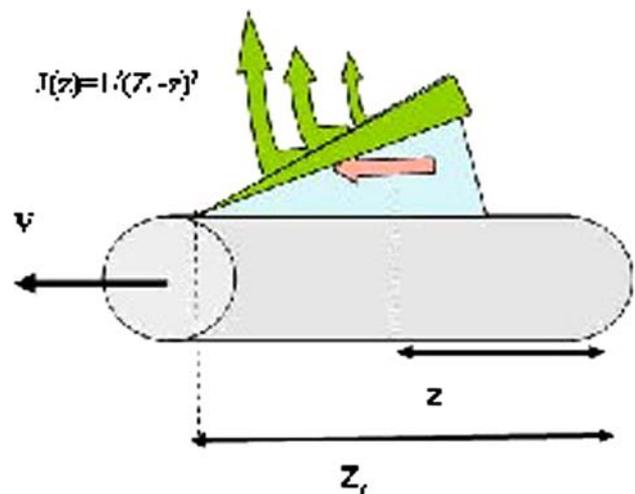
$$J(z) \propto (Z_c - z)^{-\lambda} \qquad (4)$$

Fig. 9 Mechanism of outward flow during evaporation. Vapour leaves at a rate per unit area J that depends on the vertical location z and diverges at the triple contact line location

where the exponent is $\lambda = (\pi - 2\theta_c)/(2\pi - 2\theta_c)$. As the meniscus contact angle goes to zero λ increases towards 1/2.

Structure of nano particles

Equation 4 predicts a growth power law of materials at the frontier line of a drop. A ring structure is expected with a well defined kinetic process. Experimental results shown in reference [1] are in full agreement with a growth process driven by Eq. 4. Together with a kinetic growth process obeying Eq. 4, the structure shows a well defined geometrical shape. The particle network arranges to exhibit a radial geometry (Fig. 10).

The structures obtained on conical tip do not exhibit the radial geometry shown in Fig. 10 (Fig. 11). In dipping experiments with pinned triple line, evaporation of liquid leads to a more complex hydrodynamic flow at the frontier. In particular, a surprising result is an evidence of lateral arrangment perpendicular to the expected liquid flow direction (Fig. 11).

Conclusion

The present work is an attempt to measure the specific interaction between dedicated peptidic sequences and materials. Also, it shows that an evaporating meniscus provides potential mean to self assemble nanoparticles. The evaporating flow may drive the nanoparticles to the tip and accumulate at the triple contact line of the meniscus.
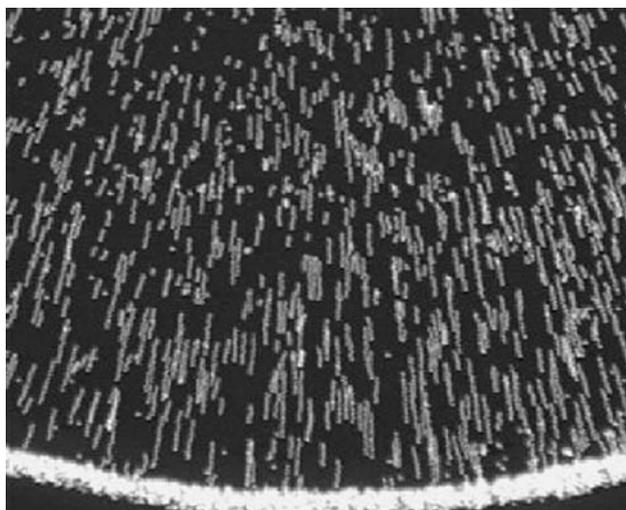

Fig. 11 Magnification on the ring structure of gold nanoparticles of diameter 10 nm. The gold nanoparticles are coated with CALNN-Si-peptide. The brightest domains indicate multi layers structures, in accordance with nanoparticles accumulation driven by an evaporating flow. The nanoparticles are mostly aligned in direction perpendicular to the radius of the ring

Fig. 10 A ring stain and a demonstration of the physical processes involved in production of such a stain. production of such a stain. The ring stain is obtained from a 2-cm-diameter drop of coffee containing 1wt% solids. Multi exposures of spheres are superimposed to indicate the motion of the microspheres. (figure extracted from reference [1])
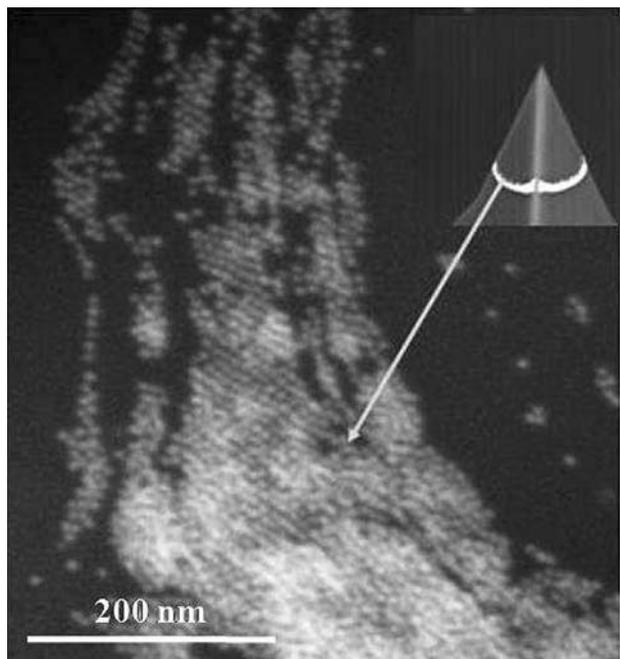
Dipping of hydrophobic conical tips show distinctely two different patterns. The structure of the pattern depends on the peptidic sequences coating the nanoparticles. For nanoparticles coated with the oligopeptides selected to interact with silica, the ring structures are formed at the location of the triple line. This case corresponds to weak interaction between the nanoparticles and the hydrophobic tip. When the tip is dipped in an aqueous solution of nanoparticles coated with oligopeptides selected to interact with carbon, there is no evidence of a ring structure but an homogeneous covering of nanoparticles on the wet part of the tip. Therefore, in itself the structure of the deposit evidences the strength of the interaction between the nanoparticles and the tip. In the latter case, the strength of the interaction between nanoparticles and substrate overcomes the laminar flow. Companion studies of the dynamical behavior of the meniscus provide an additional information giving a coherent picture of the whole process. Beside these original patterns related to the specific sequence of the peptides, the next step and the main objective is to control the attachment of nanoparticles on carbon nanotubes. The first results, partly presented in the present work, are very much encouraging showing the specific interaction on Multi Walled and Single Walled carbon nanotubes.

References

1. R.D. Deegan, O. Bakajin, T.F. Dupont, H. Greb, S.R. Nagel, T.A. Witten, Nature **389**(6653), 827–829 (1997)
2. S. Moosman, G.M. Homsy, J. Colloid. Interface Sci. **73**, 212–223 (1980)
3. R.D. Deegan, O. Bakajin, T.F. Dupont, H. Greb, S.R. Nagel, T.A. Witten, Phys. Rev. E **62**, 756–765 (2000)
4. Y. Sun, G.C. Walker, J. Phys. Chem. B **106**, 2217–2223 (2002)
5. E.R. Dufresne, E.J. Corwin, N.A. Greenblatt, J. Ashmore, D.Y. Wang, A.D. Dinsmore, J.X. Cheng, Phys. Rev. let. **91**, 224501–224504 (2003)
6. D.T. Wasan, D. Nikolov Alex, Nature **423**, 156–159 (2003)
7. Q.L. Zhang, S. Gupta, T. Emrick, T.P. Russel, J. Am. Chem. Soc. **128**, 38–98 (2006)
8. B.P. Khanal, E.R. Zubarev, Angew. Chem. Int. Ed. **46**, 2195–2198 (2007)
9. C. Jai, J.P. Aime, D. Mariolle, R. Boisgard, F. Bertin, Nano Letters **6**(11), 2554–2560 (2006)
10. F.J. Brochard, J. Chem. Phys. **84**, 4664 (1986)
11. D. Quéré, J.M. Di Meglio, F. Brochard-Wyart, Rev. Phys. Appl. **23**, 1023 (1998)
12. R. Lévy, T.K.T. Nguyen, R.C. Doty, I. Hussain, R.J. Nichols, D.J. Schirin, M. Brust, D.G. Fernig, JACS **126**, 10076–10084 (2004)
13. R.R. Naik, L.L. Brott, S.J. Clarson, M.O. Stone, J. Sci. Nanotechnol. **2**, 95–100 (2002)
14. M.J. Pender, L.A. Sowards, J.D. Hartgerink, M.O. Stone, R.R. Naik, Nano. Lett. **6**, 40–44 (2006)
15. L. Marty, V. Bouchiat, C. Naud, M. Chaumont, T. Fournier, A.M. Bonnot, Nano. Lett. **3**, 1115–1118 (2003)
16. L. Marty, A. Iaia, M. Faucher, V. Bouchiat, C. Naud, M. Chaumont, T. Fournier, A.M. Bonnot, Thin Sol. Films **501**, 299 (2006)
17. H.J. Dai, J.H. Hafner, A.G. Rinzler, D.T. Colbert, R.E. Smalley, Nature **384**, 147–150 (1996)
18. C.V. Nguyen, K.J. Chao, R.M.D. Stevens, D. Delzeit, A. Cassel, J.D. Harper, J. Han, M. Meyyapan, Nanotechnology **12**, 363 (2001)
19. R. Stevens, C. Nguyen, A. Cassel, L. Delzeit, M. Meyyappan, J. Han, Appl.Phys.Lett. **77**, 3453–3455 (2000)
20. C. Jai, J.P. Aimé, R. Boisgard, Dynamical properties of an evaporating nanomeniscus. submitted.
21. C. Bernard, al. Competition between hydrodynamic forces at nanometer scale and the strength of the specific interaction between peptides and materials. in preparation (2007)